NLR-TP-2000-213

Thermal-Gravitational Modelling and Scaling of Heat Transport Systems for Applications in Different Gravity Environments: Super-Gravity Levels & Oscillating Heat Transfer Devices

A.A.M. Delil

20010627 079

REPORT DOCUMENTATION PAGE

Form Approved OMB No. 0704-0188

1. AGENCY USE ONLY (Leave blank)	2. REPORT DATE	3. REPORT TYPE AND DATES COVERED
	16 May 2000	Conference Report, 1-13 July 2000

4. TITLE AND SUBTITLE

Thermal-Gravitational Modelling and Scaling of Heat Transport Systems for Applications in Different Gravity Environments: Super-Gravity Levels & Oscillating Heat Transfer Devices

5. FUNDING NUMBERS

6. AUTHOR(S)

A.A.M. Delil

7. PERFORMING ORGANIZATION NAME(S) AND ADDRESS(ES)

National Aerospace Laboratory NLR, Amsterdam, The Netherlands

9. SPONSORING/MONITORING AGENCY NAME(S) AND ADDRESS(ES

NLR

10. SPONSORING/MONITORING AGENCY REPORT NUMBER

NLR-TP-2000-213

11. SUPPLEMENTARY NOTES

Text in English, 18 pages, 42 references.
Also available for download at the NLR homepage
http://www.nir.nl/public/library/index.html.

12a. DISTRIBUTION/AVAILABILITY STATEMENT

Approved for public release. Distribution is unlimited.

12b. DISTRIBUTION CODE

ABSTRACT (Maximum 200 words)

Several publications describe research carried out at NLR on the thermal-gravitational modelling and scaling of two-phase heat transport systems for spacecraft applications. They dealt with mechanically and capillary pumped two-phase loops. The activities pertained to pure geometric, pure fluid to fluid, or hybrid scaling between a prototype system and a model at the same gravity level, and between a prototype in micro-gravity and a model on earth. Recent publications also include scaling aspects of a prototype loop for a Moon or Mars base application and a terrestrial model. The work discussed here was carried out in the last couple of years. It concerns scaling to super gravity levels, and was done because a promising super-gravity application for (two-phase) heat transport systems can be the cooling of high power electronic in spinning satellites and in military aircraft. In such aircraft, power electronics can be exposed, during manoeuvres, to transient accelerations up to say 12 g (120 m/s^2). The discussions include pulsating two-phase loops and also oscillating (pulsating) heat transfer devices, for which several important applications in different acceleration environments have been identified.

14. SUBJECT TERMS

NLR, Dutch, Thermal-Gravitational Modelling, Heat transport systems, Gravity environments, Hybrid scaling, Super-gravity levels, Pressure drop, Heat transfer equations

15. NUMBER OF PAGES

16. PRICE CODE

17. SECURITY CLASSIFICATION OF REPORT	18. SECURITY CLASSIFICATION OF THIS PAGE	19. SECURITY CLASSIFICATION OF ABSTRACT	20. LIMITATION OF ABSTRACT
UNCLASSIFIED	UNCLASSIFIED	UNCLASSIFIED	UL

DOCUMENT CONTROL SHEET

	ORIGINATOR'S REF. NLR-TP-2000-213		SECURITY CLASS. Unclassified

ORGINATOR
National Aerospace Laboratory NLR, Amsterdam, The Netherlands

TITLE
Thermal-Gravitational Modelling and Scaling of Heat Transport Systems for Applications in Different Gravity Environments: Super-Gravity Levels & Oscillating Heat Transfer Devices

PRESENTED AT
30th International Conference on Environmental Systems and 7th European Symposium on Space Environmental Control Systems, Toulouse, France, 10-13 July 2000.

AUTHORS A.A.M. Delil	DATE 16 May 2000	pp 18	ref 42

ABSTRACT
Several publications describe research carried out at NLR on the thermal-gravitational modelling and scaling of two-phase heat transport systems for spacecraft applications. They dealt with mechanically and capillary pumped two-phase loops. The activities pertained to pure geometric, pure fluid to fluid, or hybrid scaling between a prototype system and a model at the same gravity level, and between a prototype in micro-gravity and a model on earth. Recent publications also include the scaling aspects of a prototype loop for a Moon or Mars base application and a terrestrial model.

The work discussed here was carried out in the last couple of years. It concerns scaling to super-gravity levels, and was done because a promising super-gravity application for (two-phase) heat transport systems can be the cooling of high power electronics in spinning satellites and in military aircraft. In such aircraft, power electronics can be exposed, during manoeuvres, to transient accelerations up to say 12 g (120 m/s^2). The discussions include pulsating two-phase loops and also oscillating (pulsating) heat transfer devices, for which several important applications in different acceleration environments have been identified.

NLR-TP-2000-213

Thermal-Gravitational Modelling and Scaling of Heat Transport Systems for Applications in Different Gravity Environments: Super-Gravity Levels & Oscillating Heat Transfer Devices

A.A.M. Delil

Division: Space

Issued: 16 May 2000

Classification of title: Unclassified

Contents

1 Tables
17 Figures

(18 pages in total)

2000-ICES-106

Thermal-Gravitational Modelling and Scaling of Heat Transport Systems for Applications in Different Gravity Environments: Super-Gravity Levels & Oscillating Heat Transfer Devices

A.A.M. Delil
National Aerospace Laboratory NLR, Space Division
P.O. Box 153, 8300 AD Emmeloord, The Netherlands
Phone +31 527 248229, Fax +31 527 248210, adelil@nlr.nl

ABSTRACT

Several publications describe research carried out at NLR on the thermal-gravitational modelling and scaling of two-phase heat transport systems for spacecraft applications. They dealt with mechanically and capillary pumped two-phase loops. The activities pertained to pure geometric, pure fluid to fluid, or hybrid scaling between a prototype system and a model at the same gravity level, and between a prototype in micro-gravity and a model on earth. Recent publications also include the scaling aspects of a prototype loop for a Moon or Mars base application and a terrestrial model.

The work discussed here was carried out in the last couple of years. It concerns scaling to super-gravity levels, and was done because a promising super-gravity application for (two-phase) heat transport systems can be the cooling of high power electronics in spinning satellites and in military aircraft. In such aircraft, power electronics can be exposed, during manoeuvres, to transient accelerations up to say 12 g (120 m/s^2). The discussions include pulsating two-phase loops and also oscillating (pulsating) heat transfer devices, for which several important applications in different acceleration environments have been identified.

INTRODUCTION AND SCALING APPROACH

Many examples of the scaling of two-phase flow and heat transfer can be found in the power industry and in the process industry. The scaling of physical dimensions is of principal interest in the process industry, where large-scale industrial systems are studied by reduced scale laboratory model systems. The scaling of the working fluid is of principal interest in the power industry. There, large-scale industrial systems (characterised by high heat fluxes, temperatures, and pressures) are translated in full size systems, operating at lower temperature, heat flux and pressure levels (e.g. the scaling of a high pressure water-steam system by a low pressure refrigerant system of the same geometry).

The thermal/gravitational modelling and scaling of two-phase heat transport systems was carried out at NLR:
- For a better understanding of two-phase flow and heat transfer phenomena.
- To provide means for comparison and generalisation of data.
- To develop a useful tool to design two-phase systems and components, in order save money and to reduce costs.

The main objective of scaling space-oriented two-phase heat transport systems and system components is the development of reliable spacecraft systems, of which the reduced gravity performance can be correctly predicted using results of terrestrial experiments with scale models.

Scaling of spacecraft systems can be useful also:
- For in-orbit technology demonstration. The performance of spacecraft heat transport systems (prototypes) can be predicted using the outcomes of in-orbit experiments on models with reduced geometry or different working fluid.
- To define in-orbit experiments to isolate a typical phenomenon to be investigated (e.g. the exclusion of gravity-induced disturbing buoyancy effects on alloy melting, diffusion and crystal growth) for a better understanding of the physical phenomena.

The magnitude of the gravitational scaling varies with the objectives, from:
- 1 g to 10^{-6} g (random direction) for the terrestrial scaling of orbiting spacecraft.
- 1 g to 0.16 g for Moon base systems, to 0.4 g for Mars base systems.
- 10^{-2} g or 10^{-6} g to 1 g for isolating gravity-induced disturbances on physical phenomena investigated.
- Low-g to another or the same low-g level in low-g aircraft or sounding rockets.
- 1 g to say 12 g, for electronics cooling in military aircraft, characterised by (transient) super-gravity conditions.

NLR developments originally pertained to the scaling of mechanically and capillary pumped two-phase loops for use in microgravity (Refs. 1 to 7). The activities were extended to applications in Moon and Mars bases (Ref. 8). Modelling and scaling activities of the last two years focus on mechanically and capillary pumped two-phase loops and oscillating heat transport devices for use in transient super-gravity environments, encountered during military aircraft manoeuvres. Similar activities are reported to be currently carried out elsewhere (Refs. 9, 10).

It is recalled from the aforementioned publications that even in single-phase systems, scaling is anything but simple, since flow and heat transfer is equivalent in the model and the original (prototype) only if the corresponding velocity, temperature fields and pressure fields are identical. Dimensionless numbers can be derived either from the conservation equations (mass, momentum and energy) or from similarity considerations, based on dimension analysis. The aforementioned identity of velocity, temperature and pressure fields is obtained if all dimensionless numbers are equal in model and prototype.

Scaling two-phase systems is far more complicated as:
− In addition to the above fields, the spatial density distribution (void and flow pattern) is to be considered.
− Geometric scaling often has no sense, e.g. bubble size or surface roughness hardly depend on system dimensions.
− Of the proportion problem, arising from the high power density levels, being typical for two some characteristic dimensions, e.g. bubble size and two-phase flow and (boiling) heat transfer.

The approach starts by summarising the results of modelling and scaling the mechanically or capillary pumped two-phase loop, shown in figure 1 (as example).
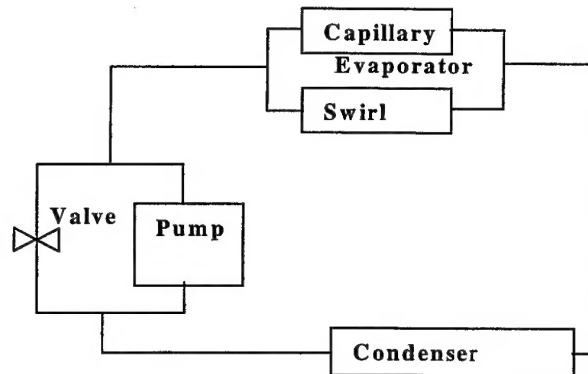

Figure 1. Two-phase loop layout

Conclusions for super-gravity conditions will be drawn from this summary A re-appraisal of the dimensionless numbers and equations has to identify those relevant to model and scale oscillating heat transfer devices.

DIMENSIONLESS NUMBERS & SIMILARITY ISSUES

Similarity considerations (for details see Refs. 1, 2) led to the identification of 18 dimensionless groups (so-called π-numbers), considered crucial for the thermal-gravitational scaling of two-phase loops. This set of 18 π-numbers, in literature called "the complete list of scaling parameters" (Ref. 11), is shown in the first column of Table 1. The other columns show the different sections of the two-phase heat transport system, depicted in figure 1: Pure liquid lines (with and without heat exchange), capillary or swirl evaporators, vapour or two-phase lines, and condensers. For each section it is indicated by • whether a typical π-number is relevant in that section.

Table 1. Relevance of π-numbers for thermal-gravitational scaling of two-phase loops	Liquid Parts		Evaporators Swirl & Capillary	Non-liquid Lines Vapour/2-Phase	Condensers
	Adiabatic	Heating/Cooling			
$\pi_1 = D/L$ = geometry	•	•	•	•	•
$\pi_2 = Re_l = (\rho v D/\mu)_l$ = inertia/viscous	•	•	•	•	•
$\pi_3 = Fr_l = (v^2/gD)_l$ = inertia/gravity	•	•	•	/•	•
$\pi_4 = Eu_l = (\Delta p/\rho v^2)_l$ = pressure head/inertia	•	•	•	•	•
$\pi_5 = \cos \nu$ = orientation with respect to g	•	•	•	/•	•
$\pi_6 = S$ = slip factor = v_v/v_l			•	•	•
π_7 = density ratio = ρ_v/ρ_l			•	•	•
π_8 = viscosity ratio = μ_v/μ_l			•	•	•
$\pi_9 = We_l = (\rho v^2 D/\sigma)_l$ = inertia/surface tension			•	/•	•
$\pi_{10} = Pr_l = (\mu Cp/\lambda)_l$		•	•		•
$\pi_{11} = Nu_l = (hD/\lambda)_l$ = convection/conduction		•	•		•
$\pi_{12} = \lambda_v/\lambda_l$ = thermal conductivity ratio			•		•
$\pi_{13} = Cp_v/Cp_l$ = specific heat ratio			•		•
$\pi_{14} = \Delta H/h_{lv}$ = Boil = enthalpy nr. = X = quality		•	•	•	•
$\pi_{15} = Mo_l = (\rho_l \sigma^3/\mu_l^4 g)$ = capillarity/buoyancy			•	/•	•
$\pi_{16} = Ma = v/(\partial p/\partial \rho)_s^{1/2}$			•	•	•
$\pi_{17} = (h/\lambda_l)(\mu_l^2 g)^{1/3}$			•		•
$\pi_{18} = L^3 \rho_l^2 \, g \, h_{lv}/\lambda_l \mu_l (T-T_o)$			•		•

There is perfect similitude between model and prototype if all dimensionless numbers are identical in prototype and model. Only then scaling is perfect. It is evident that this is not possible for two-phase flow and heat transfer: the phenomena are too complex, the number of important parameters or π-numbers is too large. Fortunately also imperfect (distorted) scaling can give useful results (Ref. 12). Therefore a careful estimation of the relative magnitudes of the different effects is required. Effects, identified to be of minor importance, make the requirement for identity of some π-numbers superfluous for the problem involved. Examples for two-phase systems are: the Mach number is not important for incompressible liquid flow, the Froude number is not important in pure vapour flow.

Further it can be remarked that, in scaling two-phase heat transport systems, geometric distortion is not permitted to study boundary layer effects and boiling heat transfer, as there has to be surface roughness identity in prototype and model. But geometric distortion is a must when the length scaling leads to impractical small (capillary) conduits in the model, in which the flow phenomena basically differ from flow in the full size prototype.

Sometimes it is more convenient to replace quality X by the volumetric vapour fraction (void fraction) α, according:

$$(1 - \alpha)/\alpha = S\ (\rho_v\ /\rho_l\ )\ X\ /(1- X)\ . \tag{1}$$

It is clear that the presented set of π-numbers is rather arbitrary, e.g. several numbers contain only liquid properties. These can be easily transferred into vapour properties containing numbers using π_6 to π_8. Similarly π_1 can be used to interchange a characteristic length (duct length, bend curvature radius) and some characteristic diameter (duct diameter, hydraulic diameter, but also surface roughness or bubble diameter). Sometimes it will even be convenient to simultaneously consider two geometric π_1-numbers. One concerns the overall channel (channel diameter versus length or bend curvature radius). The second pertains to other parameters as the ratio of surface roughness and bubble diameter to investigate boiling heat transfer, or the ratio of surface roughness and channel diameter to study friction pressure drop.

The best scaling approach is to choose (combinations of) π-numbers such that they optimally suit the problem under investigation, e.g.:
- The Morton number Mo,

$$\pi_{15} = \text{Mo}_l = \text{Re}_l^4\, \text{Fr}_l/\text{We}^3 = \rho_l\, \sigma^3/\mu_l^4\, g, \tag{2}$$

  which is useful for scaling two-phase flow with respect to gravity, as it contains only liquid properties, surface tension and gravity.
- The Mach number Ma,

$$\pi_{16} = \text{Ma} = v/(\partial p/\partial \rho)^{1/2}, \tag{3}$$

  which is a crucial quantity, if the compressibility is important, because choking depends on the vapour quality of the two-phase mixture.

- The enthalpy or boiling number

$$\pi_{14} = \text{Boil} = \Delta H(z)/\ h_{lv} = Q/\ \dot{m}h_{lv}\ . \tag{4}$$

Q is the power fed to the boiling liquid. This number appears in the expression for the dimensionless enthalpy at any z in a line heated from outside (q is the heat flux):

$$\pi_{14} = \Delta H(z)/h_{lv} = \Delta H_{in}/h_{lv} + \pi Dzq/\dot{m}h_{lv}\ . \tag{5}$$

For sub-cooled or heated liquid this is

$$\pi_{14} = Q/\dot{m}\ Cp_l\ \Delta T, \tag{6}$$

ΔT being the temperature drop. The above implies that, if the dimensionless entrance enthalpies are equal for different fluids flowing in a similar geometry, equality of the boiling number ensures equal non-dimensional enthalpies at all similar axial locations. For thermodynamic equilibrium conditions this means equal qualities at similar locations, and similar sub-cooling and boiling lengths.
- The condensation number, in which h is the local heat transfer coefficient,

$$\pi_{17} = (h/\lambda_l)\ (\mu_l^2/g\ \rho_l^{\ 2})^{1/3}. \tag{7}$$

- The vertical wall condensation number, with T_o as the local sink, T as the local saturation temperature.

$$\pi_{18} = L^3\rho_l^{\ 2}\ g\ h_{lv}/\mu_l\ \lambda_l(T- T_o)\ . \tag{8}$$

A first step in a practical approach to scale two-phase heat transport systems is identification of important phenomena, to obtain π-numbers for which identity in prototype and model must be required to realise perfect scaling according to the so-called Buckingham pi theorem (crucial in similarity considerations). Distortion will be permitted for π-numbers pertaining to less important phenomena. Important phenomena and the relevant π-numbers will be different in different parts of a system. As said before, the relevance of the π-numbers in the various loop sections is indicated by • in Table 1 (π-numbers for thermal-gravitational scaling of two-phase loops.

For refrigerants, like ammonia and R114, forced convection heat transfer overrules conduction completely. Therefore π_{10}, π_{11} and π_{12}, are not critical in gravitational scaling. π_{16} can be neglected also as the system maximum power level and line diameters correspond with flow velocities far below the sonic velocity in all system parts.

Considering π_3/π_5, it can be remarked that inertia overrules buoyancy not only in pure vapour flow or in a low gravity environment, but also for horizontal liquid sections on earth ($v \rightarrow \pi/2$). This implies that there is π-number identity for these sections in the low-g prototype and in the terrestrial model, for a horizontal arrangement of these sections. Also it is remarked that, in the porous (liquid) part of a capillary-pumped evaporator, surface tension (σ/D_p) is

dominant over inertia ($\pi_9 \rightarrow 0$): hence the evaporator exit quality will approach 1 (pure vapour). This means that gravity is less important for the vapour part of the evaporator and the vapour line to the condenser.

A first conclusion, that can be drawn now, is: Condensers and, in mechanically pumped systems, also two-phase lines, are crucial in scaling with respect to gravity. They set conditions for evaporators and single-phase sections. A second conclusion is: In adiabatic two-phase lines of mechanically pumped systems in low-gravity, only shear forces will cause separation of phases in a high-quality mixture. This leads to annular flow (a fast moving vapour in the core and a, by frictional drag induced, slowly moving liquid annulus at the inner line wall) for the lower flow rates. For increasing power, hence flow rate, the slip factor will increase introducing waves on the liquid-vapour interface and entraining of liquid droplets in the vapour: wavy-annular-mist flow. A similar flow pattern can be predicted for vertical downward flow on earth, as it easily can be derived from the flow pattern map for downward two-phase flow shown in figure 2 (Ref. 13). In this figure, water properties at 20 °C must be used to determine the scale of the abscissa. The Froude number for two-phase flow used in this figure is defined as:

$$Fr_{tp} = (16\,\dot{m}^2/\pi^2 D^5 g)[X^2/\rho_v^2 + (1-X)^2/\rho_l^2] . \qquad (9)$$

$$\boxed{\begin{aligned} Mo_w &= \frac{\rho_w\,\sigma_w^3}{g\,\mu_w^4} \\ \rho_w &= 10^3\ kg/m^3 \\ \mu_w &= 10^{-3}\ Ns/m^2 \\ \sigma_w &= 7.3 \times 10^{-2}\ N/m \\ g &= 9.8\ m/s^2 \\ Fr_{tp} &= \frac{v_{tp}^2}{gD} = \frac{16\,m^2}{\pi^2 gD^5}\left[\frac{(1-X)^2}{\rho_l^2} + \frac{X^2}{\rho_v^2}\right] \end{aligned}}$$
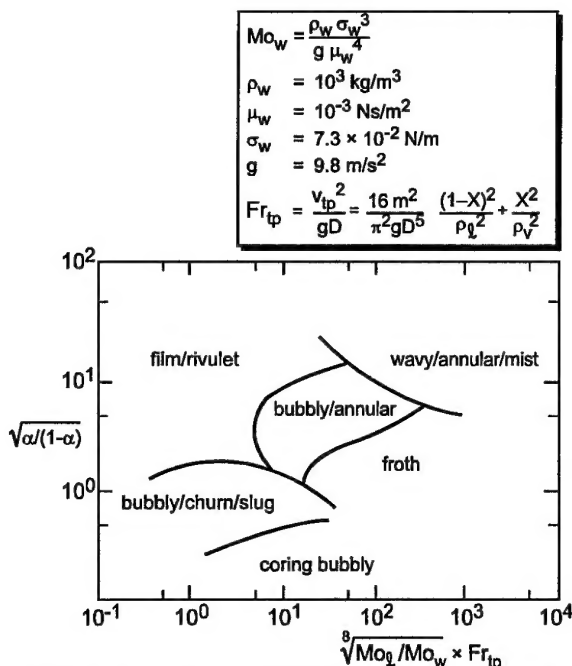

Figure 2. Flow pattern map (vertical downward flow)

Comparing low-g and vertical downward terrestrial flow one has to account in the latter for the reduction of the slip factor by the gravity forces assisting the liquid layer flowing down (draining effect). Anyhow, vertical down flow is the preferred two-phase line orientation in the terrestrial model, because of its axial-symmetric flow pattern.

A similar conclusion can be drawn for the straight tube condenser. In condensers the flow will change from wavy annular mist to pure liquid flow, passing several flow patterns, depending on the path of the condensation.

Consequences of scaling are elucidated by the figures 3 and 4, showing the temperature dependence of $g.Mo_l = \rho_l.\sigma^3/\mu_l^4$ and $(\sigma/\rho_l)^{\frac{1}{2}} = D.g^{\frac{1}{2}}/(We/Fr)^{\frac{1}{2}} = D.g^{\frac{1}{2}}/(E\ddot{o})^{\frac{1}{2}} = D.g^{\frac{1}{2}}/2(E\ddot{o})^{\frac{1}{2}}$. Eötvös number Eö and Bond number Bo are:

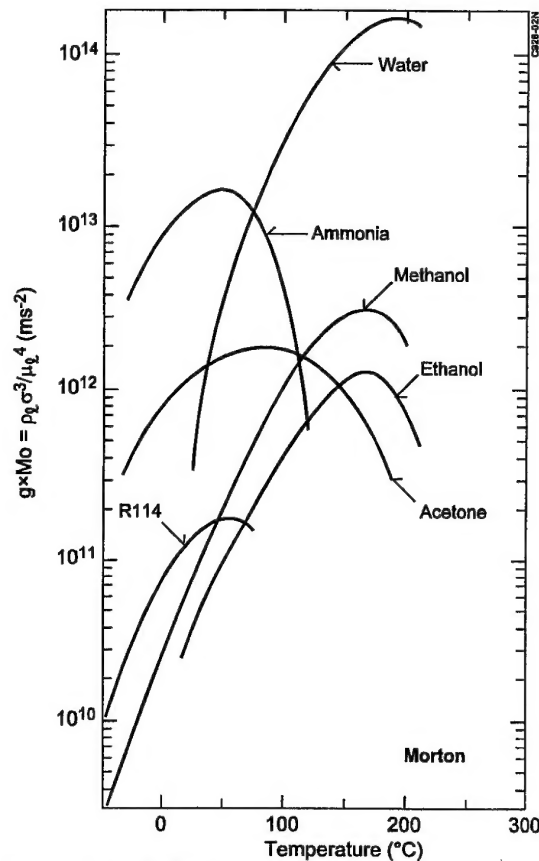$$E\ddot{o} = 4\ Bo = g\ D^2\ (\rho_l - \rho_v)/\ \sigma . \qquad (10)$$

Figure 3. $\rho_l.\sigma^3/\mu_l^4$ versus temperature for some fluids

The conclusions on scaling possibilities were drawn from figures like the figures 3 and 4 in earlier publications (Refs. 1 to 8). They pertain to scaling at the same gravity level or to scaling of a prototype in a lower than 1-g environment, and a model on earth, preferably operating in the vertical down-flow (gravity assist) mode.

They can be summarised by:
- Scaling two-phase heat transport systems is very complicated. Only distorted scaling offers some possibilities, when not the entire loop but only loop sections are involved.
- Scaling with respect to gravity is hardly discussed in literature. Some possibilities can be identified for very limited, typical conditions only.

- Scaling at the same gravity level can cover only a limited range. Scaling of high-pressure system (parts), e.g. ammonia at 110 °C, by low-pressure system (parts), e.g. -50 °C ammonia, might be attractive either for safety reasons or to reduce the impact of earth gravity in vertical two-phase sections. It follows from the figures, that the length scale ratio between high-pressure prototype and low-pressure model (both characterised by $\rho_l \sigma^3/\mu_l^4 = 2.10^{12}$ m/s^2) is $L_p/L_m = [(\sigma/\rho_l)_p/\sigma/\rho_l)_m]^{1/2} \approx 0.4$. Anticipating later discussions, it is remarked that in low temperature vertical down flow on earth the impact of gravity is minimised, hence it is suitable to simulate conditions below 1-g.
- Scaling with respect to gravity is restricted to say two decades, if the prototype and model fluid is the same.
- Scaling a full size low-gravity (< 10^{-2} g) mechanically-pumped R114 loop, like the ESA mechanically pumped Two-Phase Heat Transport System, can be adequately done by NLR's ammonia test rig, since the 10^{-2} - 10^{-3} g R114 prototype and the terrestrial ammonia model have approximately identical Morton numbers. This fluid to fluid scaling leads to a length scaling $D_p/D_m = (g_m/g_p)^{1/2} * (\sigma/\rho_l)^{1/2}_p/(\sigma/\rho_l)^{1/2}_m \approx 4.5$ to 6.5, in agreement with the ratio of actual diameters: 21 mm for the R114 space prototype and 4.93 mm for the terrestrial ammonia model.
- NLR's mechanically pumped two-phase ammonia test rig offers also some opportunities to scale the TPX ammonia loops (Ref. 14).
- A very attractive scaling possibility is the scaling of a two-phase prototype for a Mars or a Moon base, by a terrestrial model with the same or a scaled working fluid. As the ratio of gravity levels between prototype and model is less than one order of magnitude (Mars 0.4, Moon 0.16), the sizes of the model have to be only slightly larger than the geometric sizes of the prototype. In addition, adjustment of the inclinations (cos ν) of non-horizontal lines in the terrestrial model may help to realise almost perfect scaling.

PRESSURE DROP & HEAT TRANSFER EQUATIONS

An important quantity is the pressure drop in the different two-phase sections considered crucial for two-phase loop modelling and scaling. The next considerations therefore will concentrate on pressure drops in condensing and adiabatic flow and restrict the discussion to straight tubes.

The total local pressure gradient for annular flow $(dp(z)/dz)_t$ is the sum of friction, momentum and gravity gradients. Following references 5 to 8, and 15 (an elaborate article on the subject), the contribution of friction is (deleting the z-dependence to shorten the notation):

$$(dp/dz)_f = -(32m^2/\pi^2\rho_v D^5)(0.045/Re_v^{0.2})[X^{1.8}+5.7(\mu_l/\mu_v)^{0.0523}*$$
$$*(1-X)^{0.47}X^{1.33}(\rho_v/\rho_l)^{0.261}+8.1(\mu_l/\mu_v)^{0.105}*$$
$$*(1-X)^{0.94}X^{0.86}(\rho_v/\rho_l)^{0.522}] . \quad (11)$$

X is local quality X(z). Re_v is the Reynolds number
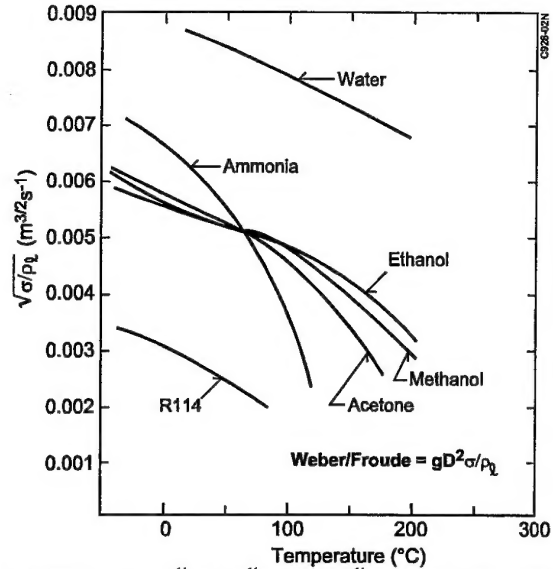
$$Re_v = 4m/\pi D\mu_v . \quad (12)$$

Figure 4. $(\sigma/\rho_l)^{1/2} = D.g^{1/2}.(We/Fr)^{-1/2}$ **versus temperature, for various fluids**

Fluid properties are assumed independent of z, since they depend only on the mixture temperature, which usually is almost constant in adiabatic and condensing sections.

The momentum constituent can be written as

$$(dp/dz)_m = -(16m^2/\pi^2 D^4)\{[2X(1-\alpha)/\rho_v\alpha^2 - \beta(1-X)/\rho_l\alpha+(1-\beta)*$$
$$*(1-X)/\rho_l(1-\alpha)+(1-X)/\rho_l(1-\alpha)](dX/dz)+$$
$$- [X^2(1-\alpha)/\rho_v\alpha^3+(1-X)^2/\rho_l(1-\alpha)^2](d\alpha/dz)\}. (13)$$

α is the z-dependent local void fraction $\alpha(z)$. $\beta = 2$ for laminar liquid flow, 1.25 for turbulent flow.

The gravity constituent is

$$(dp/dz)_g = (1-\alpha)(\rho_l-\rho_v)g \cos\nu. \quad (14)$$

$g \to 0$ for microgravity conditions and $g \cos\nu$ equals 9.8 m/s^2 for vertical down flow on Earth, 3.74 m/s^2 for vertical down flow on Mars and 1.62 m/s^2 on the Moon. α is eliminated in (13) and (14) by inserting (1).

Slip factor S is to be specified. The principle of minimum entropy production (Ref. 16) yields

$$S = [(1+1.5Z)(\rho_l/\rho_v)]^{1/3} . \quad (15)$$

This is for annular flow, in which the constant Z (according to experiments) is above 1 and below 2.

$$S = \{(\rho_l/\rho_v)[1+Z'(\rho_v/\rho_l)(1-X)/X]/[1+Z'(1-X)/X]\}^{1/3} \quad (16)$$

for real annular-mist flow, annular flow with a mass fraction Z' of liquid droplets entrained in the vapour. Z' is between 0 (zero entrainment) and 1 (full entrainment). In the limiting cases $Z \to 0$ and $Z' \to 0$, (15) and (16) reduce to

$$S = (\rho_l/\rho_v)^{1/3} . \quad (17)$$

This represents ideal annular flow. It will be used here for simplicity reasons and since it allows comparison with the results of calculations found in literature. The influence of $Z \neq 0$ and $Z' \neq 0$ is interesting for future investigations.

Inserting (17) into (1) and (11, 13, 14), yields

$$(dp/dz)_m = -(32\dot{m}^2/\pi^2\rho_v D^5).(D/2).(dX/dz)\ [2(1-X)(\rho_v/\rho_l)^{2/3} + \\ +2(2X-3+1/X)(\rho_v/\rho_l)^{4/3} + (2X-1-\beta X)(\rho_v/\rho_l)^{1/3} + \\ + (2\beta-\beta X-\beta/X)(\rho_v/\rho_l)^{5/3} + 2(1-X-\beta+\beta X)(\rho_v/\rho_l)]. \quad (18)$$

$$(dp/dz)_g = (32\dot{m}^2/\pi^2\rho_v D^5)\{1-[1+(\rho_v/\rho_l)^{2/3}\ (1-X)/X]^{-1}\}* \\ *[\pi^2 D^5 g\ cosv(\rho_l-\rho_v)\rho_v/32\dot{m}^2]. \quad (19)$$

To solve (11, 18, 19) an extra relation is necessary, defining the z-dependence of X. A relation often used,

$$dX/dz = -X_{entrance}/L_c , \quad (20)$$

(L_c = condensation length). But this means uniform heat removal (hence linear quality decrease along the duct), which is unrealistic. It is better to use

$$\dot{m}\ h_{lv}(dX/dz) = -h\pi D[T(z)-T_s] , \quad (21)$$

relating local vapour quality and heat transfer. h is the local heat transfer coefficient h(z), for which we can write

$$h = 0.018(\lambda_l\rho_l^{1/2}/\mu_l)Pr_l^{0.65}|-(dp/dz)_t|^{1/2} D^{1/2}, \quad (22)$$

assuming that the major thermal resistance is in a laminar sub-layer of the turbulent condensate film (Ref. 15).

As already mentioned the two-phase flow path is almost isothermal, which implies constant temperature drop $T(z) - T_s$ (for a constant sink temperature T_s), constant fluid properties and a constant Prandtl number, defined by

$$Pr_l = Cp_l\ \mu_l\ /\lambda_l . \quad (23)$$

The total condensation pressure drop is

$$\Delta p_t = \int_0^{L_c} (dp/dz)_t dz . \quad (24)$$

The equations (1, 11, 18, 19, 21, 22) can be combined. This yields an implicit non-linear differential equation in the variable X(z), which can be rewritten into a solvable standard form for differential/algebraic equations

$$F(dX/dz, X) = 0. \quad (25)$$

Figure 5 compares the pressure gradient constituents for ammonia vertical down-flow at two temperatures. The curves prove that the impact of gravity decreases with decreasing temperature. This confirms the earlier statement that low-gravity behaviour can be simulated the best by terrestrial down-flow tests at low temperature.

Modelling and calculations were extended from adiabatic to condensing flow in a straight duct (Refs.17, 18), in order to investigate the impact of gravity level on the duct length

required to achieve complete condensation. This impact, reported to lead to duct lengths being more than one order of magnitude larger for zero gravity, as compared to horizontal orientation on earth (Ref. 19), was assessed for various mass flow rates, duct diameters and thermal (loading) conditions, for ammonia and R114. A summary of results of calculations for ammonia is presented next. To compare the results of calculations with data from literature, the condenser in reference 19, was chosen as the baseline. Main characteristics are: power 1 kW, line diameter 16.1 mm, ammonia temperature 300 K and temperature drop to sink 10 K. The gravity levels considered are: zero gravity g=0, Earth gravity (1-g) g=9.8 m/s^2, Mars gravity g=3.74 m/s^2, Moon gravity g=1.62 m/s^2, and 2-g super-gravity 19.6 m/s^2. Illustrative results of calculations are discussed next.
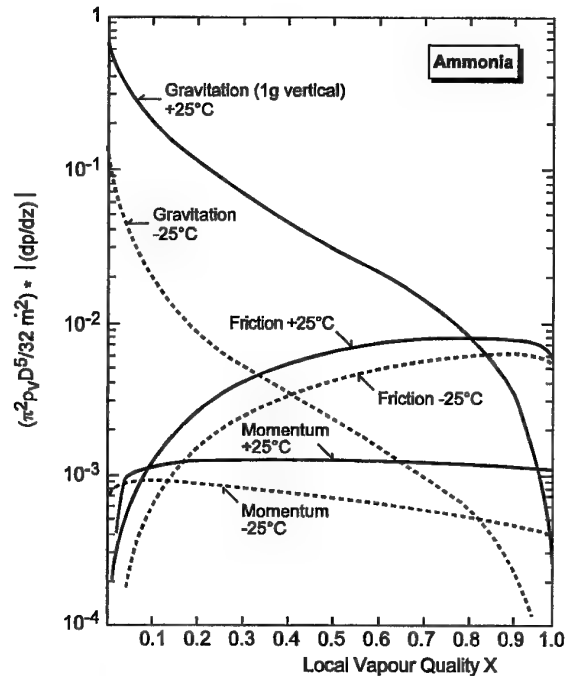

Figure 5. Pressure gradient constituents as function of vapour quality, for ammonia at +25°C and -25°C

Figure 6 depicts the vapour quality X along the condensation path (as a function of non-dimensional length z/D) for all gravity levels mentioned, including the curves for zero-g and horizontal condensation on earth, found in literature (Ref. 19). From this figure it can be concluded that: the length required for full condensation strongly increases with decreasing gravity. Zero-gravity condensation length is roughly 10 times the terrestrial condensation length. The data of reference 19 clearly can be considered as extremes.

To assess the impact of the saturation temperature on condensation, similar curves were calculated for two other temperatures, 243 K and 333 K, and the above parameter values. They indicate that the full condensation length

increases with temperature for zero-g conditions, but decreases with temperature for other gravity levels. This implies that differences between earth gravity and low-g decrease with decreasing temperature. It confirms the remark that gravity impact is smaller at lower temperatures.
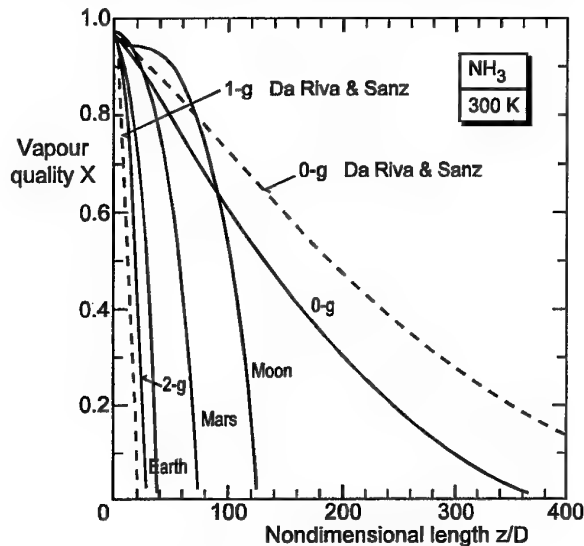

Figure 6. Vapour quality along the reference duct

Calculations of the vapour quality distribution along the 16.1 mm reference duct for condensing ammonia (at 300 K) under Earth gravity and 0-g conditions, for power levels ranging from 0.5 kW up to 25 kW, yielded (Ref. 17) that:
- A factor 50 in power, 25 kW down to 500 W, corresponds in a zero gravity environment to a relatively minor reduction in full condensation length, i.e. from 600 D to 400 D (9.5 to 6.5 m).
- Under earth gravity conditions, power and full condensation length are strongly interrelated: from L_c = 554 D at 25 kW to only 19 D at 500 W.
- The gravity dependence of the full condensation length decreases with increasing power, until the differences vanish at roughly 1 MW condenser choking conditions. The latter value is an upper limit, calculated (Ref. 16) for ideal annular flow. Choking may occur at considerably lower power values in the case of actual annular-wavy-mist flow, but the value exceeds anyhow the choking limit for homogeneous flow, roughly 170 kW.

Calculation of the vapour quality along the duct for three gravity levels (0, Earth and 2-g) and three duct diameters (8.05, 16.1 and 24.15 mm) at 300 K, yielded the ratio of the absolute duct lengths $L_c(m)$ needed for full condensation under zero-g and one-g respectively (Ref. 17). It has been concluded that the ratio between full condensation lengths in zero-g and on Earth ranges from roughly 1.5 for the 8.05 mm duct, via 11 for the 16.1 mm duct, up to more than 30 for the 24.15 mm duct. In other words, small line diameter systems are less sensitive for differences in gravity levels as compared to larger diameter systems. This has been confirmed by TPX I flight data (Ref. 20).

As the model developed is mainly valid for annular flow, it will be worthwhile to investigate the impact of other flow patterns inside the condenser duct (mist flow at high quality, slug and bubbly flow at low quality and wavy-annular-mist in between). In other words, it is to investigate whether the pure annular flow assumption, leads towards slightly or substantially overestimated full condensation lengths. Complications are that the boundaries flow patterns are not accurately known and flow pattern transitions strongly depend on temperature and line diameter. Accurate knowledge of the gravity level dependent two-phase flow regimes is crucial for modelling and designing two-phase heat transport systems for space, as flow patterns directly affect thermal hydraulic characteristics of two-phase flow and heat transfer. Therefore flow pattern (regime) maps are to be created, preferably in the non-dimensional format (Fig. 2) or in the 3-dimensional format of the figures 7 and 8, presenting data measured with a R12, 10.5 mm line diameter two-phase loop during many K135 aircraft flights (Ref. 21). Such flow pattern maps can then be used to determine, in an iterative way, via the flow pattern dependent constitutive equations for two-phase flow and heat transfer, the actual trajectories of condensing or evaporating (boiling) flow. The latter will finally lead to an accurate determination of the pressure drops in the various sections and of the heat transfer in the evaporator or condenser sections of a two-phase heat transport system.
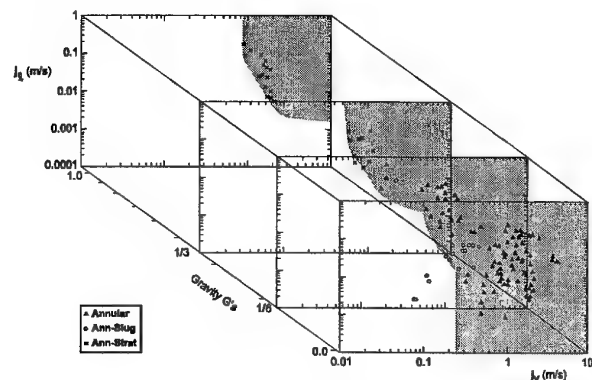

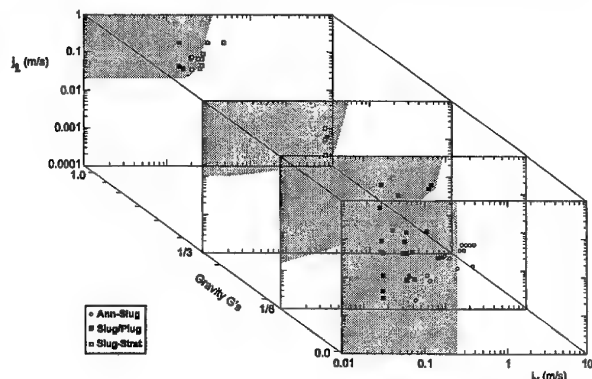**Figure 7. Annular flow: Gravity dependent 3-D map**

Figure 8. Slug/plug flow: Gravity dependent 3-D map

Figure 9 qualitatively illustrates the aspects of pressure gradient characteristics of various flow regimes in terms of an apparent interfacial friction factor.
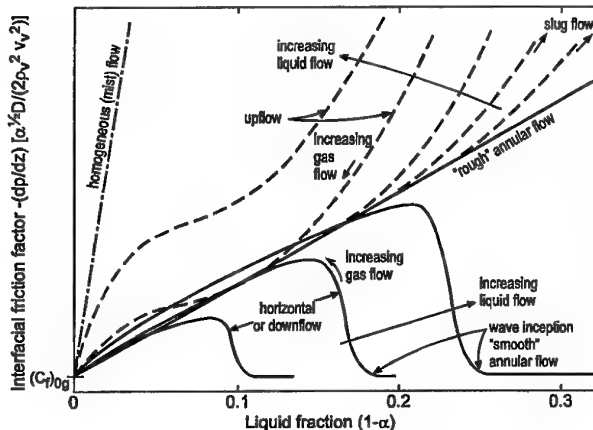

Figure 9. Qualitative aspects of pressure gradient (apparent friction factor) for various flow patterns

In summary it can be said that the information presented confirms the results of other models. When designing condensers for space applications, one should carefully use and interpret data obtained from terrestrial condenser tests, even when the latter pertain to vertical downward flow situations (characterised by the same flow pattern).

The equations given are useful for a better understanding of the problems that can be expected: e.g. the needed condenser lengths in space applications. Equations and results of the calculations suggest that hybrid scaling, which combines geometric and fluid-to-fluid scaling, can usefully support the design of space-oriented two-phase heat transport systems and their components. With respect to the local heat transfer equation used in equation (22), it is remarked that it has a wrong lower limit $h \rightarrow 0$ for $(dp/dz)_t \rightarrow 0$, which disappears by incorporating conduction via the liquid layer. Preliminary calculations indicate that incorporation of pure conduction will lead to somewhat shorter full condensation lengths, both for zero and for non-zero gravity environments. This implies only quantitative changes: Consequently the conclusions presented before remain valid.

Finally it is stressed, that the design of ammonia two-phase heat transport system prototypes for Mars and Moon base applications, looks very promising. This is because flow pattern maps for planetary gravity levels can be easily obtained from measurements in models on earth, with the same or with another working fluid. These models will have (almost) identical geometry and (if necessary) equal lines. They also might have a dedicated inclination with respect to the Earth gravity vector (i.e. cos ν = 0.4 in the case of Mars, 0.16 in the case of the Moon). These maps can, in addition, include data obtained from experiments with ammonia test loops, carried out during low-g aircraft trajectories.

1-G SCALING OF PROTOTYPES FOR SUPER-G

The preceding considerations, pertaining to gravity-assist conditions (vertical down-flow in some gravity field), remain valid and useable for two-phase loops, including pulsating two-phase loops, in super-gravity-assist conditions.

A quantitative example is the simple extrapolation of the gravity dependent condensation curves (Fig. 6) to 12-g, which yields a 10-g gravity-assist full condensation length of the order of 10 D.

Though many things will be different in the anti-gravity mode, the general thermal-gravitational scaling rules are valid for both gravity assist and anti-gravity conditions. Two interesting scaling possibilities, directly derivable from the figures 3 and 4, are discussed hereafter.

First, ammonia is the most promising working fluid for two-phase systems operating between 270 and 350 K, e.g. for cooling electronics in a super-gravity environment around say 10-g. Water, having better performance above 350 K, is also a candidate fluid. But it can freeze when the system is not operating (which is undesirable or unacceptable). Also its performance, being under 315 K below the acetone performance, becomes even unacceptably low under 300 K.

Figure 3 yields for ammonia in the aforementioned operation range (~ 10-g at 270 - 350 K) a value of g.Mo$_l$ between 1 - 1.4$*10^{13}$. This implies that the working fluid of the terrestrial model must have a g.Mo$_l$ of 1 - 1.4$*10^{12}$. This requirement is fulfilled by acetone, within roughly the same temperature range. Figure 4 straightforwardly gives that the corresponding geometric scaling ratio between model and prototype ($L_m/L_p = D_m/D_p$) is between 3 and 3.5. The above features make acetone well suited for 1-g scale models to simulate 10-g ammonia prototypes

Secondly, if ammonia is not an acceptable working fluid (e.g. because of safety requirements) and water is not a candidate (because of the earlier mentioned reasons), acetone might be the alternative for a 10-g, 270 - 350 K prototype. Figure 3 yields that the g.Mo$_l$ of 1 - 1.4$*10^{12}$ for acetone can be adequately scaled by R114 at 1-g within the same temperature range or a slightly lower one. The corresponding geometry ratio between model and prototype ($L_m/L_p = D_m/D_p$) is about 1.5, according to figure 4. Consequently, R114 can be considered useful for 1-g scale models to simulate 10-g acetone prototypes.

ANTI-GRAVITY ISSUES

The impact of anti or against gravity or super-gravity can be assessed by recalling figure 6, showing the absolute values of the three pressure drop constituents. The results of pressure drop calculations, presented in the preceding sections, pertained to gravity-assist condensation This implies that the calculations were done for cosν = +1, meaning (as it is gravity-assist) that the contribution of gravity had the opposite sign of the constituents of friction and momentum.

The results, of the only calculations for a case where the gravitational acceleration was against the flow direction of the two-phase mixture, are depicted in figure 10.
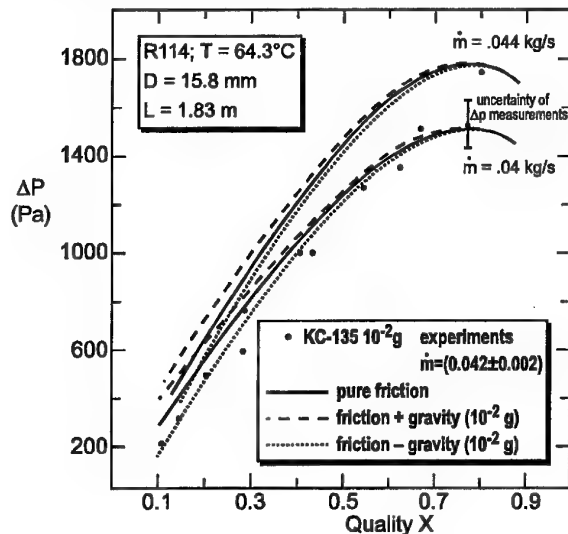

Figure 10. Measured versus calculated adiabatic pressure drops in a R114 duct

The figure depicts the flight data (Ref. 22) and three curves: one with the acceleration in the flow direction, one against the flow direction, and one perpendicular to the flow. The latter were considered to be extremes, as only the gravity level (10^{-2}g) was published, not the direction. Though 10^{-2}g is only a small acceleration, the curves clearly illustrate an impact of reversal of the direction of gravity. It is obvious that this impact will be orders of magnitude larger at super-gravity levels.

The above suggests that useful anti-gravity performance calculations can be carried out. But one shall keep in mind that the equations used pertain to annular flow only.

When considering anti-(super)-gravity modes, four important issues are to be noted:
– First, any pump of a two-phase system has to deliver a pumping pressure that is at least the sum of all pressure losses in the systems. In an anti-10g mode, this is mainly the gravitational pressure drop. Figure 5 illustrates that the contributions of friction and momentum become negligible, as compared to the 12-g contribution, which can by obtained by simply shifting the 1-g curve one decade upwards. The 10-g curve clearly overwhelms the curves of the other constituents, for almost all vapour qualities except for qualities over say 0.9, where the flow pattern probably will be homogeneous, instead annular. In case of a mechanical pump, the huge (super-gravity) pressure losses can be overcome by the use of a correctly designed displacement pump. Existing capillary pumped systems, however, will fail completely, since existing capillary structures can operate a two-phase loop against gravity, only if the maximum pumping

height to be delivered is less than say 6 metres. The 6 m gravitational pressure drop is at least a factor 20 smaller than the 10-g super-gravity pressure drops. Current high-performance capillary pumps use reasonably permeable wicks with a pore size of 0.5 μm to realise the 6 metres pumping height. For a 20 times larger pumping height, the pore size shall be about 25 nm. But a wick of such small pores will not have the required permeability of a capable capillary pump. Consequences for vapour pressure driven two-phase systems, like oscillating (pulsating) heat transport devices, will be discussed in a later section.
– Second, the pressure and temperature drops are only minor in the gravity-assist condensation curves presented. It means that the condensation is almost isothermal, hence the fluid properties can be assumed constant. This will not be the case for anti-super-gravity conditions, meaning that for the latter conditions calculations will become very complicated.
– Third, for super-g conditions there is no information at all on flow pattern maps and the boundaries between the different flow regimes. Therefore and as it is expected that the various items will substantially differ from the (hardly available) existing 1-g ones, the creation of consistent flow pattern maps for the super-gravity environment has been started at NLR.
– Fourth, gravity influences the pressure drop and the corresponding temperature drop across the heat transport system. This is confirmed by experimental data (Ref. 9): Compared to 0-g pressure and temperature drops, the drops decrease with increasing gravity-assist, and increase with increasing anti-gravity.

SINGLE-PHASE OSCILLATING HEAT TRANSFER

The assessment of super-gravity performance issues of oscillating (pulsating) heat transfer devices starts with the description of a very interesting device (Fig. 11), following a short earlier presented summary (Ref. 23).

For detailed discussions on this synchronised forced oscillatory flow heat transfer device, it is referred to the publications of the originators (Refs. 24-26) and to other publications on this device and on the related phase-shifted forced oscillatory flow heat transfer devices (Ref. 27).

The device is not a two-phase device but a single-phase one. The set-up consists of two reservoirs at different temperatures, connected by a 0.2 m long, 12.7 mm inner diameter acrylic tube, containing 31 glass capillaries with an inner diameter d = 1 mm. The open cross-sectional area of the capillary structure, including the triangular sections between the capillaries, A_l was determined to be 67 mm^2, being 53% of the total inner cross-sectional area of the tube (A = 127 mm^2) The reservoirs are equipped with flexible membranes. A variable frequency shaker is used to oscillate the incompressible working liquid inside the capillary structure. The frequency f is variable from 2 and 8 Hz. The tidal displacement Δz is variable from 20 to 125 mm.

The operation is as follows. Starting with the capillary structure filled with hot liquid, this liquid is replaced, in the first half of the oscillation period, by liquid from the cold reservoir, but with the exception of the thin (Stokes) boundary layer. Heat is then exchanged very effectively in radial direction between the hot Stokes layer and the cold core. Heat accepted by the core is removed to the cold reservoir in the second half of the oscillation period. The heat flow, via the liquid, between the reservoirs equals

$$Q = \lambda_{eff} \, (A_l/L) \, \Delta T = \rho_l \, Cp_l \, \kappa_{eff} \, (A_l/L) \, \Delta T. \tag{26}$$

ΔT is the temperature difference between the hot and cold reservoir. κ_{eff} is the effective thermal diffusivity , λ_{eff} is the effective thermal conductivity.
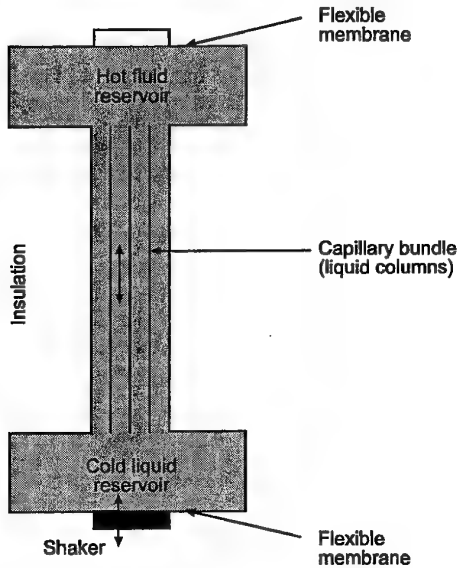

Figure 11. Synchronised forced oscillatory flow heat transfer device

Figure 12 shows the experimentally determined effective thermal diffusivity as a function of tidal displacement and oscillation frequency, for a device with glass capillaries and water as working fluid. The solid lines are analytical predictions from the laminar theory. The figure indicates that the effective thermal conductivity via the liquid is

$$\lambda_{eff} = B \, \rho_l \, Cp_l \, \{(\Delta z)^2 / (d/2)\} \, (2\pi f \, \mu_l/\rho_l)^{1/2}. \tag{27}$$

Proportionality factor B, the tangent of the straight lines in figure 10, can be written as (Refs. 24, 26)

$$B = 2^{-5/2} \, Pr_l^{-1} \, \{B' + B'' - B'B'' \, (1 + Pr_l^{1/2}) \, * \\ *\{Pr_l^{-1/2} - 2 \, (1 + Pr_l)\})\} \, . \tag{28}$$

$$B' = Pr_l / (Pr_l - 1), \tag{29}$$

$$B'' = \{(1 - B') \, (Pr_l \, \kappa_l / \kappa_{wall})^{1/2} - B' \, \lambda_l / \lambda_{wall})\} \, * \\ * \, \{\lambda_l / \lambda_{wall} + (\kappa_l / \kappa_{wall})^{1/2}\}^{-1}. \tag{30}$$
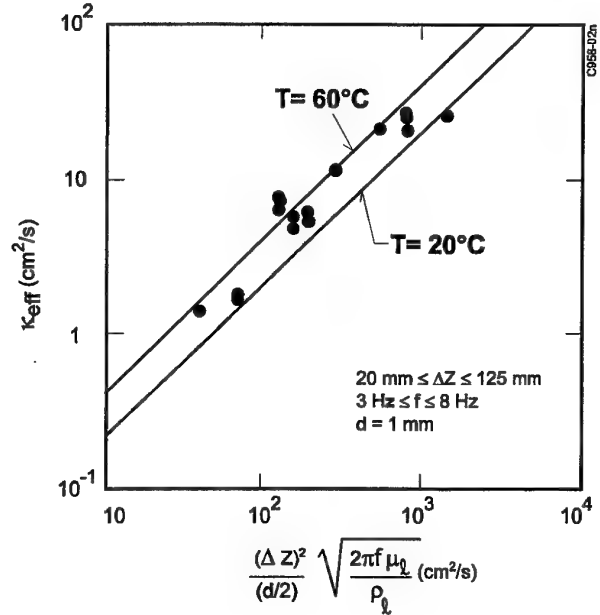

Figure 12. Effective thermal diffusivity

An important conclusion for future design activities can be drawn by considering the equations (28) to (31): The highest values of proportionality factor B occur for small Prandtl number fluids and walls which are good thermal conductors (Ref. 24).

An alternative representation is obtained by defining an enhancement (proportionality) factor E for undeveloped oscillating flow in synchronised systems

$$(\lambda_{eff} / \lambda_l) \, -1 = (\kappa_{eff} / \kappa_l) \, -1 = (Pr_l \, \Delta z \, /2d)^2.E \, . \tag{31}$$

E depends on the dimensionless Womersley number

$$Wo_l = (d/2) \, (2\pi \, f \, \rho_l / \mu_l)^{1/2} \, . \tag{32}$$

It can be approximated by

$$E = Wo_l^4 \, / \, 24 \qquad \text{for} \qquad Wo_l << 1 \, , \tag{33}$$

$$E = Wo_l \, (Wo_l - 2^{-1/2} \,) \qquad \text{for} \qquad Wo_l << 1 \, . \tag{34}$$

Figure 13 shows the enhancement factor E as a function of Womersley number, for decades of the Prandtl number: 0.1, 1 and 10 (Refs. 25, 28).

Inserting properties of water at 20 °C, d = 1 mm, Δz = 125 mm and f = 8 Hz (hence Pr_l = 6.9 and Wo_l = 3.55), yields (according to figure 13) for the above synchronised device an enhancement factor 0.14. The corresponding λ_{eff} (about $1.2 * 10^4$ W/m.K) means a power density slightly above $3 * 10^6$ W/m². This is confirmed by the experimental data: $2.9*10^6$ W/m² for a gradient of 280 K/m (Ref. 24). The total effective thermal conductivity is roughly 5000 W/m.K, if it is based on the total cross-sectional tube area, including the insulating glass walls.
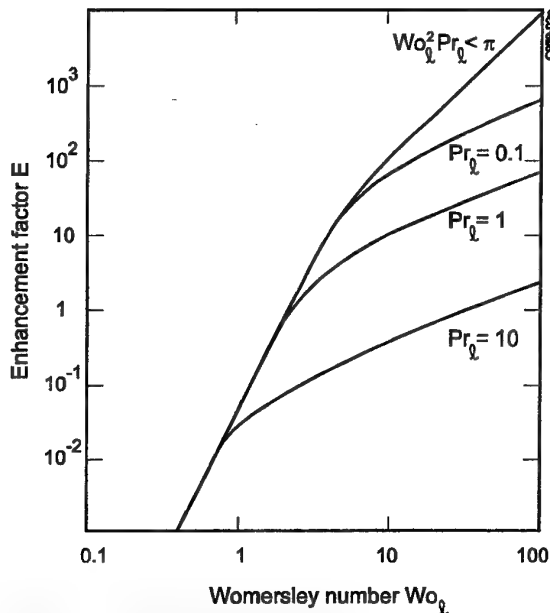
Figure 13. Enhancement factor E as a function of Womersley number Wo_l and Prandtl number Pr_l

A similar expression has been derived for undeveloped oscillating flow in phase-shifted systems (Refs. 27, 29):

$$\lambda_{eff} = \lambda_l \{1 + 0.707 (1 + Pr_l^{-1})^{-1} (1 + Pr_l^{-1/2})^{-1}\} * $$
$$* \{(\Delta z)^2/(d/2)\}\{(2\pi f \rho_l Cp_l/\lambda_l)^{1/2}\} . \quad (35)$$

Inserting the properties of water at 20 °C, d = 1 mm, Δz = 125 mm and f = 8 Hz yields λ_{eff} = 2.5*10^4 W/m.K, being 2.5 times the value of the corresponding synchronised forced oscillatory flow heat transfer device.

Disadvantages of the concepts are the poor current state of the art and the power consumption of the shaker. The latter, estimated to be more than 5 W in the described cases, strongly increases with oscillation frequency and tidal displacement. A disadvantage for some micro-gravity applications can be the noise introduced by the shaker.

The major advantage of the concepts is its variable conductance, which is adjustable via the frequency and tidal displacement from almost zero (liquid in rest in a poorly conductance structure) to values comparable to or even better than heat pipes. This makes such devices very useful for instance to drain huge amounts of thermal power from a hot vessel for nuclear reactor cooling, in case of an emergency.

OSCILLATING TWO-PHASE HEAT TRANSFER

Two oscillating two-phase heat transfer devices can be distinguished: Pulsating two-phase heat transfer loops and devices like the pulsating or meandering heat pipe and the flat swinging heat pipe. These systems have in common that the operation is driven only by the vapour pressure differences induced by the heat to be transported itself. In other words, they do not need an additional power source.

Figure 14 depicts the temperature dependent saturation pressure of some candidate working fluids. It illustrates that when designing a device, one has to select a working fluid with a high saturation pressure gradient (dp/dT) within the operating (temperature) range, as higher system pumping pressures correspond with higher dp/dT- values.
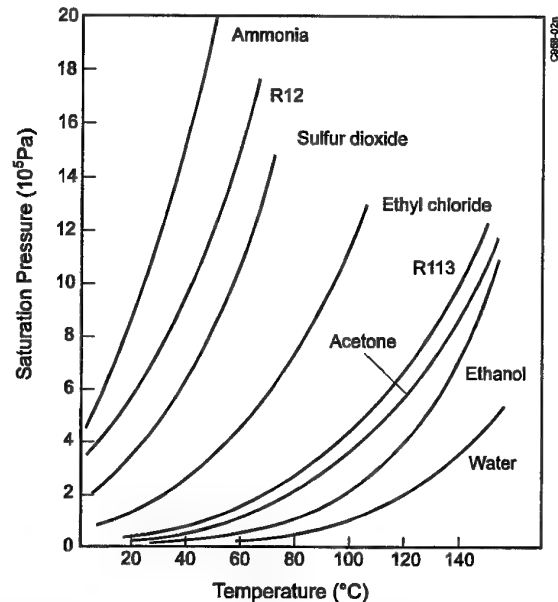

Figure 14. Vapour pressures of candidate working fluids, as a function of the temperature

PULSATING TWO-PHASE LOOPS

Pulsating two-phase heat transfer loops already were proposed many years ago (Refs. 29 to 31). These systems are just two-phase loops driven by vapour pressure differences, instead of mechanical or capillary pumping action. The vapour pressure pumping action is realised by incorporation of two one-way valves: one at the entrance, the other at the exit, of a separate unit, an evaporator or a control reservoir. Power fed to the system, increases the internal vapour pressure in the section between the two valves till the exit valve will open and the loop starts to run, also opening the second valve to let sub-cooled liquid flow into the pumping section. After some pressure decay the valves will close re-starting the process. A careful design will certainly lead to a properly performing heat transfer device. The advantages of such loops are the already mentioned driving mechanism (the heat to be transferred only, without an additional power), the high heat transport capability, their self-priming capability, and their capability to work against gravity. A disadvantage is the pulsating operation, hence pulsating heat and mass transfer, accompanied by temperature variations and possibly also vibrations (g-jitter), which will make the system not attractive for some micro-gravity applications.

The majority of the remarks on two-phase thermal-gravitational modelling and scaling made up to now are

directly applicable for pulsating two-phase loops. The only new issue to be accounted for is the proper design of the desired driving pressure, which is directly coupled to the corresponding difference of the saturation temperatures in evaporator and condenser.

OTHER OSCILLATING TWO-PHASE DEVICES

Other oscillating devices have various names, e.g. bubble-driven heat transfer device (Ref. 27), pulsating or meandering heat pipe (Refs. 32, 33), capillary heat pipe or capillary tunnel heat pipe (Refs. 34, 35), flat swinging heat pipe (Ref. 36), and spirally wound or serpentine-like heat pipe (Ref. 37).
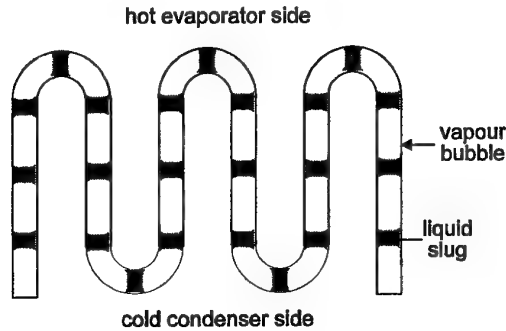

Figure 14. Schematic of an oscillating device section

Figure 14 schematically shows a section of such an oscillating device, called looped (Ref. 38) or closed-loop (Ref. 32), if the two legs at each end are not dead ends but interconnected, thus creating a closed loop configuration. If the latter configuration has a spring-like geometry like the arrangement discussed in references 38 and 39, the operation of the device has been frequently observed to stabilise after a certain start-up period, producing a periodic pumping of almost constant frequency into one direction (Ref. 39). Such behaviour is very similar to the behaviour of the just described pulsating heat transfer loops. The similarity suggest that the function of the valves in the pulsating heat transfer loops is being delivered by the stick-slip conditions of the slug-plug distribution of the working fluid inside the closed-loop spring-like meandering structure, whose heating and cooling sections have also a certain periodicity. Anyhow, the slug-plug distribution is essential for these oscillating devices, without valves.

The velocities of bubbles and slugs in a tube are governed by buoyancy, liquid inertia, liquid viscosity and surface tension forces, in the general case of bubbly or slug-plug flow in a gravity field. This means that properly chosen dimensionless groups can be very helpful to discuss the aspects of slug-plug flow in oscillating devices (Ref. 40).

First the condition of slug-plug distribution determines the maximum inner tube diameter (Refs. 40, 41, 32)

$$D_{max} = 1.836 \; g^{-1/2} \; [\sigma/(\rho_l - \rho_v)]^{1/2} \cong 1.836 \; g^{-1/2} \; (\sigma/\rho_l)^{1/2} \quad (36)$$

for $\rho_l \gg \rho_v$.

Consequently, the thermal-gravitational scaling of the inner tube diameter can be derived from figure 4.

Second, the slug-plug condition also sets the lower limit of the slug (bubble) size: It shall be at least 0.6 times the tube diameter (Ref. 38). This extra requirement has an impact on the liquid filling ratio $(1 - \alpha)$. If not fulfilled, the bubbles will be too small to maintain the slug flow pattern, characterised by high heat transfer densities. The resulting bubbly flow leads to a far less efficient heat transport.

Other useful plots of dimensionless numbers are shown in the figures 16 and 17 (Ref. 39). Figure 16 shows the dimensionless velocity v^* as a function of the Morton number Mo and the Eötvös number Eö.

$$v^* = v \; [g \; D \; (1 - \rho_v/\rho_l)]^{-1/2} \cong v / (g \; D)^{1/2} \; . \quad (33)$$
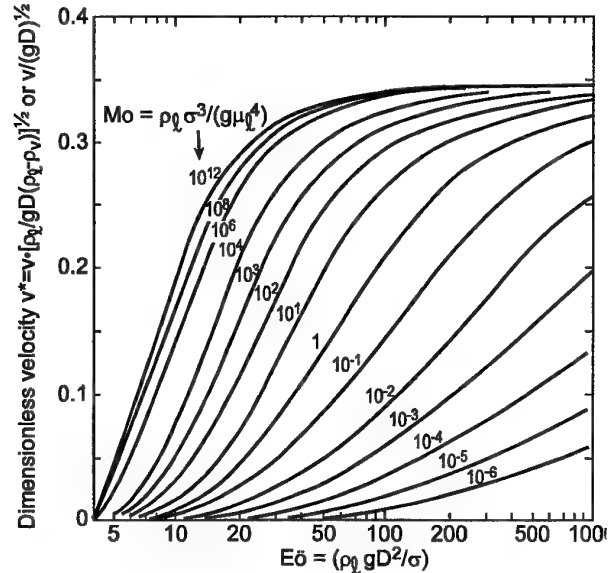
Figure 16. Dimensionless velocity v^* as a function of Morton number Mo and Eötvös number Eö

Figure 17 depicts many experimental data, but in the alternative plotting (Ref. 40) v^* as a function of the inverse viscosity number Mu, for different values of Archimedes number Ar.

The dimensionless numbers Mu and Ar are given by:

$$Mu = \mu_l \; [g \; D^3 \; (\rho_l - \rho_v) \; \rho_l]^{-1/2} \cong \mu_l \; (g \; D^3 \; \rho_l^2)^{-1/2}, \quad (37)$$

$$(Ar)^2 = Mo = (\rho_l \; \sigma^3/\mu_l^4 \; g) / (1 - \rho_v/\rho_l) \cong \rho_l \; \sigma^3/\mu_l^4 \; g \; . \quad (38)$$

The three asymptotes shown are:
- $v^* = 0.345$, for Eö > 100 and Mu $< 10^{-3}$, the inertia dominant domain.
- $v^*. \; Mu = 10^{-2}$, for Eö > 100 and Mu > 0.5, the viscosity dominant domain.
- $Mu^2. \; Ar = 0.16$ and Eö < 3.37, the surface tension dominant domain.

The last domain is the most important for the oscillating devices considered here, as Eö < 3.37 straightforwardly leads to the maximum tube diameter equation (30) and dominating surface tension means that plug-slugs do not move, if there is no (thermal) power input. In this domain slug flow is guaranteed by surface tension, if slug bubbles have diameters of at least 0.6 times the tube diameter.
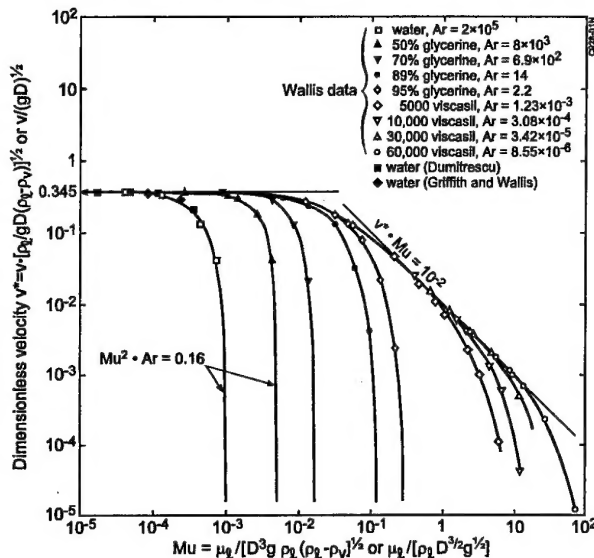

Figure 17 Dimensionless velocity v* as a function of dimensionless inverse viscosity number Mu

Some quantitative considerations on these pulsating two-phase heat transfer devices are presented next, in order to get a certain feeling for or a better understanding of how to design, scale and test such devices. Geometrical data and some performance figures of the earlier described single phase oscillating heat transfer device will be used.

EXPERIMENTAL DATA FROM LITERATURE

Several recently published results of experiments confirm the remarks made up to now. They will be summarised first, before being used to establish a simple quantitative model for oscillating (pulsating) heat transfer devices.

Super-gravity experiments were done, on a 4.5 m diameter centrifuge table, with a non-looped device, consisting of 23 turns of 0.42 m long, 1.1 mm internal diameter, stainless steel capillaries (Ref. 9). The working fluid was acetone, the liquid filling ratio $(1-\alpha)$ was 0.6. The length of the sections was 120 mm for the heating and the adiabatic section, 180 mm for the cooling section. The experiments were done in both gravity-assist and anti-gravity conditions. Experimental data confirms that gravity influences the pressure drop and the corresponding temperature drop across such devices. For example, while continuously transporting the maximum power 40 W, the finally reached stable heater section temperature increased from 130 °C in the 6-g-assist case, via 160 °C at 0-g and 185 °C at 6-g anti-gravity, to 200 °C at 12-g anti-gravity.

There occurred no evaporator dry-out for all acceleration conditions specified. The above tests, and vibration tests (frequency 0 to 16 kHz, acceleration 0 to 15 g, amplitude 0 to 7 mm, inclination 0 - 180°), showed that these oscillating devices are not sensitive for acceleration fields.

Experiments with a 4-turn, 396 mm long, glass, closed-loop meandering device showed good performance also (Ref. 27), even for capillary diameters larger than the maximum diameter D_{max} (see equation 36). But poor performance was observed for diameters below 0.6 D_{max}.

Results of experiments with a 2.4 mm diameter tube test device showed for all liquids a maximum performance at a liquid filling ratio $(1-\alpha)$ around 0.35. For filling ratios up to 0.8, the performances are slightly below these maximum performances, above 0.8 they strongly decrease. Typical values of the performance are about 1.25 W/K for water and 0.8 W/K for ethanol and R141b, for a temperature drop of 50 K, within the working range 10 - 100 °C. The total wall resistance of the heating and cooling sections were calculated to be 1.25 K/W per tube.

A typical periodic vapour-plug propagation phenomenon was reported to occur in a 10-turn water system (Ref. 32): 2.5 Hz for a temperature drop of 30 K and for the very high liquid filling $1-\alpha = 0.95$.

DEFINITION OF PULSATING DEVICES FOR TESTING

A first step in a logic approach to develop useful pulsating two-phase test devices is to dimension these such that test outcomes can directly be compared to the presented performance data of the described synchronised oscillating single-phase device.

A second step is to assume that the single-phase device (Fig. 11) consists of 85 identical cylindrical channels with an average internal diameter d = 1 mm. This represents the actual configuration of 31 glass capillaries (1 mm ID) and 54 triangular channels present between these capillaries, thus yielding the total liquid cross-sectional area $A_l = 85*\pi/4 \approx 67$ mm². For simplicity reasons the tube length is assumed to be equal to the displacement length: $L = \Delta z = 125$ mm. The power transported by each of these capillaries can be calculated from the data presented. For the maximum transport case, being for frequency f = 8 Hz and temperature difference $\Delta T = 56$ K, this becomes $(\pi/4)* d^2 *2.9*10^6 = (\pi/4) *10^{-6} \approx 2.3$ W.

The third step is the simplification to consider the pulsating two-phase device (Fig. 14) to be, in essence, a configuration of identical, parallel elements, each one transporting the same amount of power, driven by the vapour pressure difference between the heat input (evaporator) section and the cooling (condenser) section. In addition, the working fluid and dimensioning of the two-phase and single-phase devices are identical: the working fluid is water, the capillary diameter d = 1 mm, the evaporator and condenser length are $L_e = L_c = L = 125$ mm. In the first approximation, it is assumed there is no adiabatic section.

The main differences between the two devices pertain to the driving mechanism, the heat transfer processes and the heat transfer locations.

A mechanical actuator is the driver of the oscillating axial movement of the liquid in the single-phase device. Only specific heat is exchanged over the entire capillary tube length L in two sequential radial (conduction) steps. In the first half of the period, heat is transferred in radial direction from the hot fluid in the core to the thin Stokes layer (and the tube wall). In the second half of the period, this heat is moved back to the cold fluid brought into the core.

In the two-phase device heat is simultaneously exchanged in radial direction, mainly by conduction, plus some convection, at two different locations. The heat is fed via the wall to the working fluid in the hot input (evaporator) section. The heat is extracted from the fluid via the wall in the cold section (condenser). This heat transfer, via the specific heat of the liquid, looks more or less identical in the two systems. The transfer difference (i.e. two-step sequential at one location, respectively simultaneous heat addition and extraction at two different locations) suggests that it is reasonable to assume that the transported power in the two-phase case is, for $\Delta T = 56$ K, twice the value for a single-phase capillary (4.6 W). As an alternative it can also be assumed that $\Delta T = 28$ K only, at a power transport of 2.3 W.

However, there is an additional latent heat transfer contribution in the two-phase device: The heat transported via the vapour bubble that grows in the heat input section (evaporator) by evaporation of a liquid micro-layer (Ref. 38). This bubble collapses in the condenser, releasing its latent heat. The pressure difference, between the (super-heated) vapour in the evaporator and the saturated vapour in the condenser, is the driving force moving the hot liquid slug from evaporator to condenser, plus moving at the same moment a similar cold slug from condenser back to the same or a neighbouring evaporator. The power transported by latent heat can be obtained by calculating the energy needed to create 8 bubbles, of length L and diameter d, per second. Consequently one obtains $8*(\pi/4)*d^2*L*\rho_v*h_{lv} = 8*(\pi/4)*10^{-6}* 0.125 * 0.2 * 2.25* 10^6 \approx 0.45$ W, which constitutes a non-negligible contribution.

The pressure head across the capillary single-phase water system can be calculated as follows. The displacement of 125 mm at frequency 8 Hz yields a liquid velocity v = 2 m/s. For water around 300 K, the Reynolds number Re_l is around 2000, which means laminar flow. Consequently the required pressure drop is 8 kPa, according to the equation

$$\Delta p = 4 * (16 / Re_l) (L / D) (\rho_l v^2 / 2) . \tag{39}$$

In the corresponding two-phase device the required pressure difference has to be far larger, because of several reasons. In the first place twice the single-phase device mass (a hot and a cold slug) has to be moved. Secondly, this double mass has to be forced through a 180 degrees bend instead a straight channel. Further, the length of the adiabatic section (L_a) is of course, in reality, never equal to zero. Finally, the process concerns all except fully developed flow, hence there is a liquid acceleration term to be added.

To get a feeling for the magnitude of these pressure enlarging effects, the length L_a is taken to be also 125 mm ($L_a = L$), as example. This has impact on the contribution of the power transport via the latent heat of evaporation. This contribution will be around 0.9 W, since the length of each of the 8 vapour bubbles, being generated and collapsing in one second, is $L_a + L$ (hence 2L, instead L). The average liquid velocity becomes v = 4 m/s. For water around 300 K, the Reynolds number Re_l now lies around 4000, which means turbulent flow. Consequently the required pressure drop has to be calculated according to

$$\Delta p = 4 * 0.0791 \, Re^{-\frac{1}{4}} (L / D) (\rho_l v^2 / 2). \tag{40}$$

As discussed in textbooks, the effect of the two bends can be accounted for by adding an extra length of 50 D. The pressure drop can now be calculated, according to equation (40), by inserting the different parameter values and by replacing L by 2*(2L + 50 D). The result is 480 kPa. To be complete an inertia term, accounting for the acceleration of the slugs eight times per second, has to be added: $8*(\rho_l v^2 / 2)$, hence 16 kPa, yielding about 500 kPa for the pressure difference required. Consequently, it can be concluded from the water curve in figure 14, that the two-phase device has to operate at a hot section temperature of at least 80 °C, to be able to deliver the pressure drop required. The figure makes also clear that more or less comparable powers can be transported by ammonia, R12, acetone, etc. Though at comparable ΔT's, this will be realised at far lower operating temperatures, as these fluids show a steeper dp/dT-relation.

The results of the above simple approach and of the detailed modelling of the physical processes, including mass-spring simulations, currently is compared and will be compared in the near future to experimental data, resulting from further experimenting at NLR. The experimental activities include many high-acceleration experiments on a rotation table. The experiments have been, are, and will be carried out both with all-metal devices, and with all-glass devices (Ref. 36). Additional experiments will be executed using a torus-like or spring-like configuration of transparent (teflon or polyethylene) flexible tubing, equipped with a simple one-way valve to influence direction and frequency of the periodic behaviour of a closed-loop configuration. Experiments pertain to various working fluids and different locations of hot and cold sections, to different lengths of adiabatic section, to various orientations, and to different acceleration levels in various directions. Results between modelling and experimental outcomes will be subject of a publication, which is being prepared for presentation early next year (Ref. 42)

CONCLUDING REMARKS

In conclusion it can be remarked that the preceding review summarises the approach for the thermal-gravitational scaling of two-phase systems. Results of similarity

considerations are given. Modelling results are discussed, including comparison with various experimental data. The discussions concern not only gravity-assist system aspects, but also the issues of operation against gravity or super-gravity. The systems considered include capillary pumped and mechanically pumped two-phase loops, pulsating two-phase loops, and other single-phase and two-phase oscillating (pulsating) devices. A simple rationale is described, to get a (quantitative) feeling to be used for the development of pulsating devices for useful experiments.

REFERENCES

1. Delil, A.A.M., Thermal gravitational modelling and scaling of two-phase heat transport systems: Similarity considerations and useful equations, predictions versus experimental results, NLR-TP-91477, 1st European Symp. Fluids in Space, Ajaccio, France, 1991, ESA SP-353, pp. 579-599.
2. Delil, A.A.M., Two-phase heat transport systems for spacecraft – Scaling with respect to gravity, NLR-TP-89127, SAE 891467, 19th Int. Conf. on Environmental Systems, San Diego, CA, 1989, SAE Trans. J. Aerospace, 98, 1989, pp. 554-564.
3. Delil, A.A.M., Two-Phase Heat Transport Systems for Space: Thermal Gravitational Modelling and Scaling Predictions Versus Results of Experiments, ASME-JSME Forum on Microgravity Fluid Flow, Portland, OR, USA, 1991, ASME-FED-Vol. 111, pp. 21-27.
4. Delil, A.A.M., Thermal Scaling of Two-Phase Heat Transport Systems for Space: Predictions versus Results of Experiments, NLR-TP-91477, Proc. 1991 IUTAM Symp. on Microgravity Fluid Mechanics, Bremen, Germany, pp. 469-478.
5. Delil, A.A.M., On Thermal-Gravitational Modelling, Scaling and Flow Pattern Mapping Issues of Two-Phase Heat Transport Systems, NLR-TP-98268, SAE 981692, 28th International Conference on Environmental Systems, Danvers, MA, USA, 1998.
6. Delil, A.A.M., Aerospace Heat and Mass Transfer Research for Spacecraft Thermal Control Systems Development, NLR-TP-98170, Heat Transfer 1998, 11th Int. Heat Transfer Conference, Kyongju, Korea, 1998, Vol. 1, Keynote Papers, pp. 239-260.
7. Delil, A.A.M., Unsolved Aerospace Heat and Mass Transfer Research Issues for the Development of Two-Phase Thermal Control Systems for Space, Invited Lecture, Int. Workshop Non-Compression Refrigeration & Cooling, Odessa, Ukraine, 1999, pp.21-42.
8. Delil, A.A.M., Some Critical Issues in Developing Two-Phase Thermal Control Systems for Space, NLR-TP-99354, 11th Int. Heat Pipe Conference, Tokyo, Japan, 1999, Pre-prints, Vol.3, Keynote and Invited Lectures, pp. 61-79.
9. Kiseev, V.M., Zolkin, K.A., The Influence of Acceleration on the Performance of Oscillating Heat Pipe, 11th Int. Heat Pipe Conference, Tokyo, Japan, 1999, Pre-prints, Vol.2, pp. 154-158.
10. Romestant, C., Sophy, T., Alexandre, A., Dynamic of heat pipe behavior under cyclic body forces environment, 11th Int. Heat Pipe Conference, Tokyo, Japan, 1999, Pre-prints, Vol.2, pp. 1-6.
11. Issacci, F., Wang, C.S.H., Dhir, V.K., Boiling Heat Transfer and Two-Phase Flow in Microgravity: A Review, Proc. 30th National Heat Transfer Conference, Portland, OR, USA, 1995, ASME-HTD-Vol. 305, pp. 3-14.
12. Murphy, G., Similitude in Engineering, Ronald Press, New York, USA, 1950.
13. Oshinowo, T., Charles, M.E., Vertical Two-Phase Flow, Flow Pattern Correlations, Can. J. Chem. Engng., Vol. 52, 1974, pp. 25-35.
14. Delil, A.A.M., Dubois, M., Supper, W., The European Two-Phase Experiments TPX I & TPX II, NLR TP 97502, Pre-prints 10th Int. Heat Pipe Conf., Stuttgart, Germany, 1997.
15. Soliman, M. & Schuster, J.R., Berenson, P.J., A General Heat

Transfer Correlation for Annular Flow Condensation, ASME C, J. Heat transfer, 1968, 90, pp. 267-276.
16. Zivi, S.M., Estimation of Steady-State Void Fraction by Means of the Principle of Minimum Entropy Production, Trans. ASME C, J. Heat Transfer, 1964, 86, pp. 247-252.
17. Delil, A.A.M., Gravity dependence of pressure drop and heat transfer in straight two-phase heat transport system condenser ducts, NLR-TP-92167, SAE 921168, 22nd Int. Conf. on Environmental Systems, Seattle, WA, USA, 1992, SAE Trans., J. Aerospace, 101, 1992, pp. 512-522.
18. Delil, A.A.M., Gravity dependent condensation pressure drop and heat transfer in ammonia two-phase heat transport systems, NLR-TP-92121, AIAA 92-4057, National Heat Transfer Conf., San Diego, CA, 1992.
19. Da Riva, I., Sanz. A, Condensation in Ducts, Microgravity Science and Technology, 4, 1991, pp. 179-187.
20. Delil, A.A.M. et al., TPX for In-Orbit Demonstration of Two-Phase Heat Transport Technology - Evaluation of Flight & Postflight Experiment Results, NLR-TP-95192, SAE 95150, 25th Int. Conf. on Environmental Systems, San Diego, USA, 1995.
21. Hamme, T.A., Best, F.R., Gravity Dependent Flow Regime Mapping, AIP Conf. Proc. 387, Space Technology & Applications International Forum, Albuquerque, NM, USA, 1997, pp. 635-640.
22. Chen, I., et al., Measurements and Correlation of Two-Phase Pressure Drop under Microgravity Conditions, J. Thermophysics, 5, 1991, pp. 514-523.
23. Delil, A.A.M., Moveable Thermal Joints for Deployable or Steerable Spacecraft Radiator Systems, NLR-MP-87016, SAE 871460, 17th Intersoc. Conf. on Environmental Systems, Seattle, USA, 1987.
24. Kurzweg, U.H., Zhao, L., Heat Transfer by High-frequency Oscillations: A New Hydrodynamic Technique for Achieving Large Effective Conductivities, Phys. Fluids, 27, 1984, pp. 2624-2627.
25. Kurzweg, U.H., Enhanced Heat Conduction in Fluids Subjected to Sinusoidal Oscillations, Trans. ASME, J. Heat Transfer, 107, 1985, pp. 459-462.
26. Kurzweg, U.H., Lindgren, E.B., Lothrop, B., Onset of Turbulence in Oscillatory Flow at Low Womersley Number, Phys. Fluids A, 1 (12), 1989, pp. 1972-1975. Enhanced Heat Conduction in Fluids Subjected to Sinusoidal Oscillations, Trans. ASME, J. Heat Transfer, 107, 1985, pp. 459-462.
27. Nishio, S., Oscillatory-Flow Heat Transport Device, 11th Int. Heat Pipe Conference, Tokyo, Japan, 1999, Pre-prints, Vol.3, Keynote and Invited Lectures, pp. 39-49.
28. Watson, E.J., Diffusion in oscillatory pipe flow, J. Fluid Mech., 133, 1983, 233-244.
29. Tamburini, P., "T-System", Proposal of a New Concept Heat Transport System, Proc. 3rd Int. Heat Pipe Conference, Palo Alto, CA, USA, 1978, AIAA CP-784, pp. 346-353.
30. Lund, K.O., Baker, K.W., Weislogel, M.M., The Vapor-Pressure Pumped Loop Concept for Space Systems Heat Transport, (Proc. 1st Int. Conference on) Aerospace Heat Exchanger Technology 1993, Palo Alto, CA, USA, (Eds. Shah, R.K., Hashemi, A.), Elsevier, Amsterdam 1993, pp. 45-55.
31. Borodkin, A.A., Kotlyarov, E.Yu., Serov, G.P., Evaporation-Condensation Pump for Providing of Working Fluid Circulation in Two-Phase Heat Transferring System, SAE 951508, 25th International Conference on Environmental Systems, San Diego, CA, USA, 1995.
32. Hosoda, M., Nishio, S., Shirakashi, R., Meandering Closed-Loop Heat-Transport Tube (Propagation Phenomena of Vapor Plug), 5th ASME/JSME Thermal Engineering Conference, San Diego, CA, USA,1999, pp. 1-8.
33. Nishio, S., Shin, H.-T.,.Oh, S.-J., Oscillation-Controlled Heat-Transport Tubes (Effect of Transition from Laminar to Turbulent Flow on Effective Conductivity), Heat Transfer 1998, 11th Int. Heat Transfer Conference, Kyongju, Korea, 1998, Vol. 3, pp. 317-322.

34. Wong, T.N., et al., Theoretical Modelling of Pulsating Heat Pipe, 11th Int. Heat Pipe Conference, Tokyo, Japan, 1999, Preprints, Vol.2, pp. 159-163.

35. Akachi, H., Motoya, S., Maezawa, S., Thermal performance of capillary tunnel type flat heat pipe, Proc. 9th Int. Heat Pipe Conference, Albuquerque, NM, USA, 1995, LA-UR-97-1500, 1997, Vol. 1, pp. 88-96.

36. Es, J. van, Woering, A.A., High-acceleration performance of the Flat Swinging Heat Pipe, accepted for presentation at the 30th International Conference on Environmental Systems, Toulouse, France, 2000.

37. Terpstra, M., Veen, J.G. van, Heat Pipes: Construction and Applications, EUR 10925 EN, Elsevier, London, 1987.

38. Maezawa, S., et al., Thermal Performance of Capillary Tube Thermosyphon, Proc. 9th Int. Heat Pipe Conference, Albuquerque, NM, USA, 1995, LA-UR-97-1500, 1997, Vol. 21, pp. 791-795

39. Smirnov, H.F., Kuznetsov, I.O., Borisov, V.V., The approximate pulsating heat pipe theory and experiment, Int. Workshop Non-Compression Refrigeration & Cooling, Odessa, Ukraine, 1999, pp.121-125.

40. Wallis, G.B., One-dimensional Two-phase Flow, McGraw-Hill, New York, 1969

41. Bretherton, F.P., The motion of long bubbles in tubes, J. of Fluid Mechanics, 10, 1961, pp. 161-188.

42. Delil, A.A.M., Theory and design of pulsating two-phase heat transport devices, Proposed for presentation during the Conference on Thermophysics in Microgravity, Space Technology & Applications International Forum, Albuquerque, NM, USA, 2001.

NOMENCLATURE

A	area (m^2)
Ar	Archimedes number (-)
B	proportionality factor (-)
Bo	Bond number (-)
Boil	boiling number (-)
C	conductance (W/K)
Cp	specific heat at constant pressure (J/kg.K)
D	diameter (m)
d	diameter of capillary or of curvature (m)
E	enhancement factor (-)
Eö	Eötvös number (-)
Eu	Euler number (-)
Fr	Froude number (-)
f	frequency (Hz)
g	gravitational acceleration (m/s^2)
H	enthalpy (J/kg)
h	heat transfer coefficient ($W/m^2.K$)
h_{lv}	latent heat of vaporisation (J/kg)
j	superficial velocity (m/s)
L	length (m)
Ma	Mach number (-)
Mo	Morton number (-)

Mu	Inverse viscosity number (-)
$\dot{m}$	mass flow rate (kg/s)
Nu	Nusselt number (-)
p	pressure (Pa = N/m^2)
Pr	Prandtl number (-)
Q	power (W)
q	heat flux (W/m^2)
Re	Reynolds number (-)
T	temperature (K or °C)
r	radius (m)
S	slip factor (-)
t	time (s)
v	velocity (m/s)
v^*	dimensional velocity (-)
We	Weber number (-)
Wo	Womersley number (-)
X	vapour quality (-)
z	axial or vertical co-ordinate (m)

α	vapour/void fraction (volumetric) (-)
β	constant in eq. (13) (-)
δ	surface roughness (m)
Δ	difference, drop (-)
κ	thermal diffusivity (m^2/s)
λ	thermal conductivity (W/m.K)
μ	viscosity ($N.s/m^2$)
ν	angle (with respect to gravity) (rad)
π	dimensionless number (-)
ρ	density (kg/m^3)
σ	surface tension (N/m)

Subscripts

a	acceleration, adiabatic, axial
c	condenser, cold
ch	(capillary) channel
e	evaporator
eff	effective
f	friction
h	hot
I	inner
g	gravitation
l	liquid
m	momentum, model
o	reference condition, outer
p	pore, prototype
r	radial
s	entropy
t	total
tp	two-phase
v	vapour
w	water